Charge Order in the Holstein Model on a Honeycomb Lattice

Y.-X. Zhang,[1,*] W.-T. Chiu,[1] N. C. Costa,[2] G. G. Batrouni,[3,4,5,6,7] and R. T. Scalettar[1]
[1]Department of Physics, University of California, Davis, California 95616, USA
[2]Instituto de Física, Universidade Federal do Rio de Janeiro Cx.P. 68.528, 21941-972 Rio de Janeiro RJ, Brazil
[3]Université Côte d'Azur, INPHYNI, CNRS, 0600 Nice, France
[4]MajuLab, CNRS-UCA-SU-NUS-NTU International Joint Research Unit, 117542 Singapore
[5]Centre for Quantum Technologies, National University of Singapore, 2 Science Drive 3, 117542 Singapore
[6]Department of Physics, National University of Singapore, 2 Science Drive 3, 117542 Singapore
[7]Beijing Computational Science Research Center, Beijing 100193, China

(Received 1 October 2018; published 19 February 2019)

The effect of electron-electron interactions on Dirac fermions, and the possibility of an intervening spin-liquid phase between the semimetal and antiferromagnetic (AF) regimes, has been a focus of intense quantum simulation effort over the last five years. We use determinant quantum Monte Carlo simulations to study the Holstein model on a honeycomb lattice and explore the role of electron- *phonon* interactions on Dirac fermions. We show that they give rise to charge-density-wave (CDW) order and present evidence that this occurs only above a finite critical interaction strength. We evaluate the temperature for the transition into the CDW which, unlike the AF transition, can occur at finite values owing to the discrete nature of the broken symmetry.

DOI: 10.1103/PhysRevLett.122.077602

Introduction.—The synthesis of graphene, i.e., single layers of carbon atoms in a hexagonal lattice, in 2004 has led to a remarkable body of subsequent work [1,2]. One of the key elements of interest has been the Dirac dispersion relation of free electrons in this geometry, allowing the exploration of aspects of relativistic quantum mechanics in a conventional solid. "Dirac point engineering" has also become a big theme of investigation of fermions confined in hexagonal optical lattices [3].

It has been natural to ask what the effects of electron-electron interactions are on this unusual noninteracting dispersion relation. Early quantum Monte Carlo (QMC) simulations and series expansion investigations of the Hubbard model on a honeycomb lattice found a critical value of the on site repulsion $U_c \sim 4t$ for the onset of antiferromagnetic (AF) order at half-filling [4]. This stood in contrast to the extensively studied square-lattice geometry for which the perfect Fermi surface nesting and the van Hove singularity of the density of states (DOS) imply $U_c = 0$. Subsequent QMC studies refined this value to $U_c \sim 3.87$ and suggested the possibility that a gapped spin-liquid (resonating valence bond) phase exists between the weak-coupling semimetal and strong-coupling AF regimes [5], a conclusion further explored in the strong-coupling (Heisenberg) limit [6]. Yet more recent work challenged this scenario and pointed instead to a conventional continuous quantum phase transition between the semimetal and AF insulator [7–9]. Equally interesting is the possibility of unusual topological superconducting phases arising from these spin fluctuations [10–19].

Graphene itself is, in fact, only moderately correlated. First principles calculations of the on site Hubbard U yield $U_{00} \sim 9.3$ eV [20], with a nearest-neighbor hopping $t \sim 2.8$ eV, so that $U/t \sim 3.3$ is rather close (and slightly below) U_c. Longer range U_{01} interactions can lead to a rich phase diagram including charge ordered phases [12,21], especially in the semimetal phase where the Coulomb interaction is unscreened. Charge ordering may also arise when electron-phonon coupling (EPC) is taken into account [22,23]. Indeed, considering such coupling would allow an exploration of the effect of other sorts of interactions on the Dirac fermions of graphene, complementing the extensive existing literature on electron-electron repulsion.

There are a number of fundamental differences between the two types of correlations. Most significantly, the continuous symmetry of the Hubbard interaction and the AF order parameter preclude a finite 2D temperature transition. Therefore, the focus is instead on quantum phase transitions. On the other hand, in the Holstein case the charge-density-wave (CDW) order has a one-component order parameter, leading to a transition that breaks a *discrete* symmetry and, consequently, a finite critical temperature (in the Ising universality class). Precise QMC values of T_c on a square lattice were only quite recently obtained [24–26]. These build on earlier QMC studies of CDW physics in the Holstein model [27,28] and introduce an exact treatment of fluctuations into earlier mean-field calculations [29].

In this Letter, we explore the effect of electron-phonon, rather than electron-electron, interactions on the properties

of Dirac fermions, through QMC simulations of the Holstein model [30] on a honeycomb lattice. We use the charge structure factor, compressibility, and Binder ratio to evaluate the critical transition temperatures and EPC, leading to a determination of the phase diagram of the model. Taken together, these results provide considerable initial insight into the nature of the CDW transition for Dirac fermions coupled to phonons.

Model and methodology.—The Holstein model [30] describes conduction electrons locally coupled to phonon degrees of freedom,

$$\hat{\mathcal{H}} = -t\sum_{\langle \mathbf{i},\mathbf{j}\rangle,\sigma}(\hat{d}^{\dagger}_{\mathbf{i}\sigma}\hat{d}_{\mathbf{j}\sigma} + \text{H.c.}) - \mu\sum_{\mathbf{i},\sigma}\hat{n}_{\mathbf{i},\sigma} + \frac{1}{2}\sum_{\mathbf{i}}\hat{P}^2_{\mathbf{i}} + \frac{\omega_0^2}{2}\sum_{\mathbf{i}}\hat{X}^2_{\mathbf{i}} + \lambda\sum_{\mathbf{i},\sigma}\hat{n}_{\mathbf{i},\sigma}\hat{X}_{\mathbf{i}}, \quad (1)$$

where the sums on $\mathbf{i}$ run over a two-dimensional honeycomb lattice [see Fig. 1(a)], with $\langle \mathbf{i}, \mathbf{j}\rangle$ denoting nearest neighbors. $d^{\dagger}_{\mathbf{i}\sigma}$ and $d_{\mathbf{i}\sigma}$ are creation and annihilation operators of electrons with spin σ at a given site $\mathbf{i}$. The first term on the right side of Eq. (1) corresponds to the hopping of electrons, with chemical potential μ given by the second term. The phonons are local (dispersionless) quantum harmonic oscillators with frequency ω_0, described in the next two terms of Eq. (1). The EPC is included in the final term. The hopping integral ($t = 1$) sets the energy scale, with bandwidth $W = 6t$ for the honeycomb geometry.

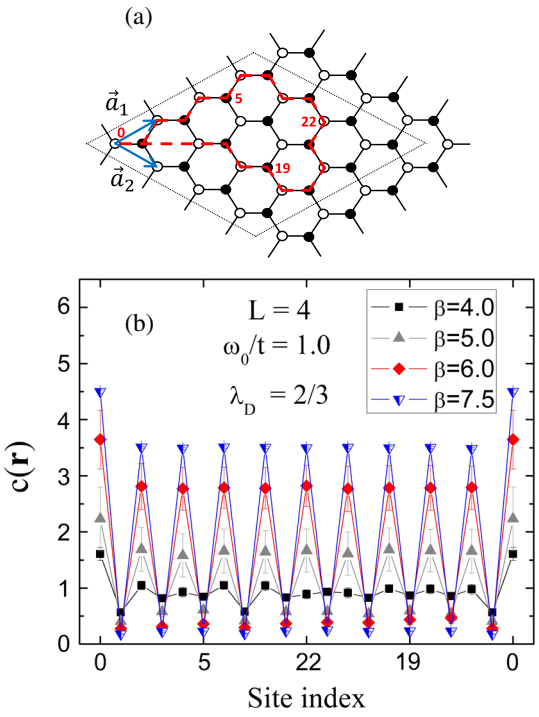

FIG. 1. (a) A 4×4 honeycomb lattice, with the trajectory (red dashed line) corresponding to the horizontal axis of (b), which shows charge correlations $c(\mathbf{r})$ at $\lambda_D = 2/3$, $\omega_0 = 1$, and several temperatures. Here, and in all subsequent figures, when not shown, error bars are smaller than the symbol size.

We use determinant quantum Monte Carlo (DQMC) simulations [31] to investigate the properties of Eq. (1). Since the fermionic operators appear only quadratically in the Hamiltonian, they can be traced out, leaving an expression for the partition function, which is an integral over the space and imaginary time-dependent phonon field. The integrand takes the form of the square of the determinant of a matrix M of dimension the spatial lattice size, as well as a "bosonic" action [32] arising from the harmonic oscillator terms in Eq. (1). The square appears since the traces over the up and down fermions are identical, which leads to a case where the minus sign problem is absent for any electronic filling.

Nevertheless, we focus on the half-filled case $\langle \hat{n}_{\mathbf{i},\sigma}\rangle = \frac{1}{2}$. This gives us access to the Dirac point where the DOS vanishes linearly. It is also the density for which CDW correlations are most pronounced. It can be shown, using an appropriate particle-hole transformation, that this filling occurs at $\mu = -\lambda^2/\omega_0^2$. We analyze lattices with linear sizes up to $L = 8$ (128 sites). By fixing the discretization mesh to $\Delta\tau = 1/20$, systematic Trotter errors become smaller than the statistical ones from Monte Carlo sampling. To facilitate the discussion, and eventual comparisons with the square-lattice case, we introduce a dimensionless EPC: $\lambda_D = \lambda^2/(\omega_0^2 W)$.

Charge ordering is characterized by the charge-density correlation function

$$c(\mathbf{r}) = \langle (n_{\mathbf{i}\uparrow} + n_{\mathbf{i}\downarrow})(n_{\mathbf{i}+\mathbf{r}\uparrow} + n_{\mathbf{i}+\mathbf{r}\downarrow})\rangle \quad (2)$$

and its Fourier transform, the CDW structure factor,

$$S_{\text{CDW}} = \sum_{\mathbf{r}}(-1)^{\mathbf{r}}c(\mathbf{r}). \quad (3)$$

The -1 phase accesses the staggered pattern of the charge ordering. The long-range behavior is investigated by performing finite-size scaling and by tracking the evolution of the insulating gap in the CDW phase.

Existence of CDW phase.—We first consider the behavior of charge-density correlations when the temperature $T = \beta^{-1}$ is lowered. Figure 1(b) displays $c(\mathbf{r})$ along the real space path of Fig. 1(a), for $\lambda_D = 2/3$, $\omega_0 = 1$, and several inverse temperatures β. When T is high ($\beta = 4$), we find $c(\mathbf{r}) \approx \rho^2 = 1$, where ρ is the density, indicating an absence of long-range order. However, an enhancement of charge correlations starts to appear at $\beta = 5$, with the emergence of a staggered pattern, which is even more pronounced at lower T, $\beta = 6$ and 7.5. This temperature evolution of real space charge correlations suggests a transition into a CDW phase.

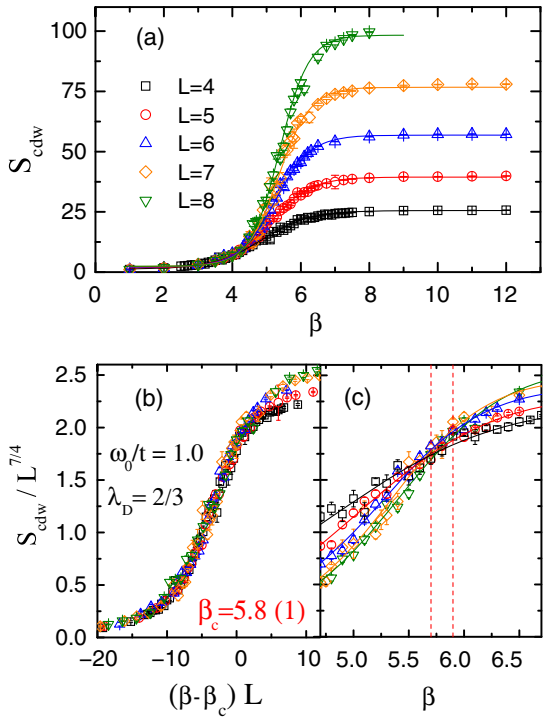

FIG. 2. (a) The charge structure factor as a function of β, for different lattice sizes ($L = 4$–8), and its (b) best data collapse, with the 2D Ising critical exponents, which yields $\beta_c = 5.8$. (c) The crossing plot for $S_{\mathrm{CDW}}/L^{\gamma/\nu}$, with vertical dashed lines indicating the uncertainty in the critical temperature. Here $\lambda_D = 2/3$ and $\omega_0 = 1$.

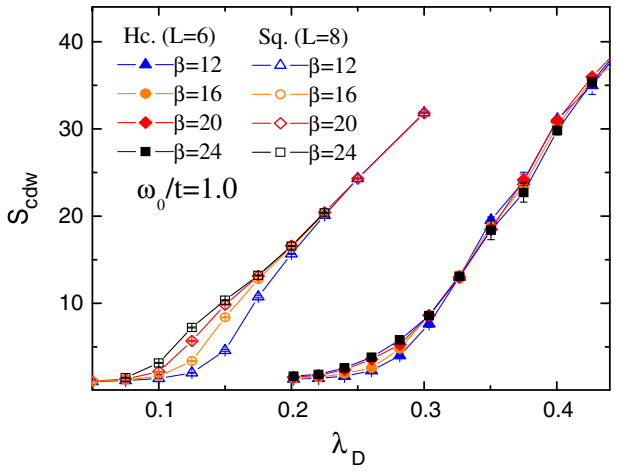

FIG. 3. CDW structure factor S_{CDW} as a function of dimensionless coupling λ_D. S_{CDW} becomes small for $\lambda_D \lesssim 0.25$. For the square lattice, S_{CDW} is large to much smaller values of λ_D. In addition, for the honeycomb (Hc.) lattice S_{CDW} does not change for the two lowest temperatures, whereas S_{CDW} continues to grow at weak coupling for the square (Sq.) lattice.

A more compelling demonstration of long-range ordering (LRO) is provided by Fig. 2(a), which exhibits the structure factor S_{CDW} as a function of β, for different linear sizes L. In the disordered phase at high T, $c(\mathbf{r})$ is short ranged and, consequently, S_{CDW} is independent of lattice size L. The emergence of a lattice size dependence of S_{CDW} and, ultimately, its saturation at a value not far from $N = 2L^2$, signals the onset temperature of LRO and a correlation length approaching the lattice size. Figure 2(a) shows that a change between these two behaviors occurs around $\beta \sim 5$–6, giving an initial rough estimate of β_c. The ground state is obtained for $\beta \gtrsim 8$; for larger values, the density correlations no longer change. The precise determination of the critical temperature T_c is accomplished by performing finite-size scaling of these data, using the 2D Ising critical exponents $\gamma = 7/4$ and $\nu = 1$, as displayed in Fig. 2(b). The best data collapse occurs at $\beta_c = 5.8(1)$, consistent with the crossing of $S_{\mathrm{CDW}}/L^{\gamma/\nu}$ presented in Fig. 2(c) and also supported by the crossing in the Binder cumulants (see Supplemental Material [33,34]). T_c for the honeycomb lattice is of the same order as that for the square lattice. For the latter at $\omega_0 = 1$, β_c ranges from $\beta_c \sim 16.7$ at $\lambda_D = 0.15$ to $\beta_c \sim 5$ at $\lambda_D = 0.27$ [25] and $\beta_c \sim 6.0$ at $\lambda_D = 0.25$ [26,38].

For the range of EPC shown in Ref. [25], β_c steadily decreases with increasing λ_D. A dynamical mean-field theory approach [39,40] found that there is a minimal β_c (maximum in T_c) for an optimal coupling strength. This nonmonotonicity is also present in the repulsive half-filled 3D Hubbard model; the AF $\beta_{\mathrm{Néel}}$ has a minimum at intermediate U. We return to this issue in what follows.

Finite critical coupling.—We investigate next how charge correlations behave as a function of the EPC and, specifically, the possibility that CDW does not occur below a critical interaction strength, as is known to be the case for the Hubbard model on a honeycomb lattice. This is a somewhat challenging question, since at weak coupling one might expect $T_c \sim \omega_0 e^{-1/\lambda_D}$ becomes small, necessitating a careful distinction between the absence of a CDW transition and T_c decreasing below the simulation temperature. Figure 3 displays the CDW structure factor as a function of λ_D at different T, on square (open symbols) and honeycomb (filled symbols) lattices, for similar system sizes. The most noticeable feature is that S_{CDW} appears to vanish for weak coupling, $\lambda_D \lesssim 0.25$, strongly suggesting a finite critical EPC for CDW order on the honeycomb lattice. This is a qualitatively reasonable consequence of the vanishing DOS at half-filling, since having a finite DOS is part of the Peierls' requirement for CDW formation [22,23,41].

To ensure this is not a finite-T effect, we contrast this behavior of S_{CDW} with that of the square lattice, for which it is believed that a CDW transition occurs at all nonzero λ_D owing to the divergence of the square-lattice DOS [25]. We note first that S_{CDW} remains large for the square lattice down to values of λ_D a factor of 2–3 below those of the honeycomb lattice. In addition, there is a distinct difference in the T dependence. In the square-lattice case, CDW correlations are enhanced as T is lowered. The S_{CDW} curves shift systematically to lower λ_D as β increases, consistent

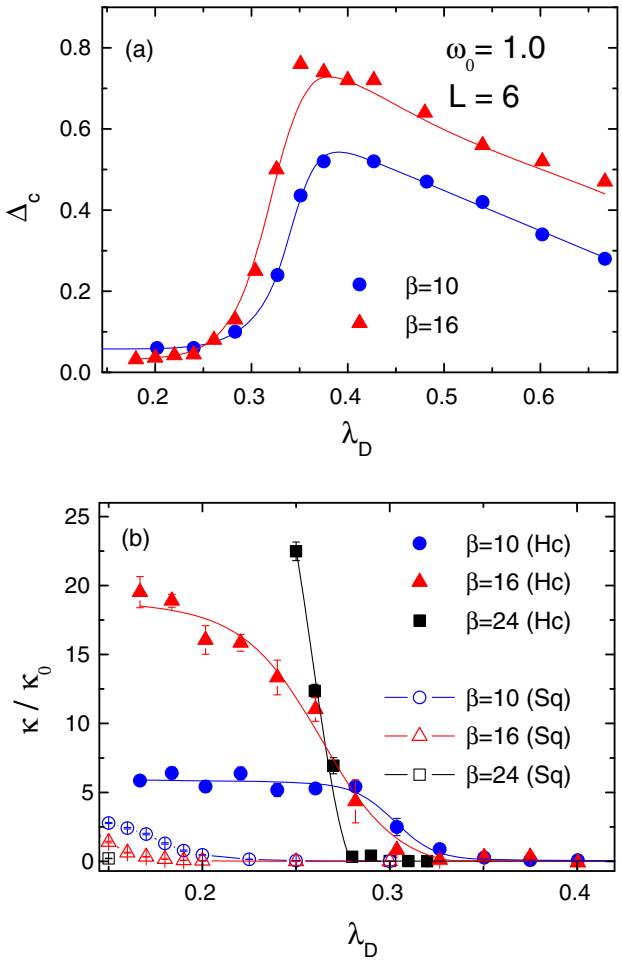

FIG. 4. (a) The charge gap Δ_c (see text) as a function of λ_D. (b) The electronic compressibility κ as a function of λ_D for square (open symbols) and honeycomb (filled symbols) lattices with linear sizes $L = 8$ and 6, respectively.

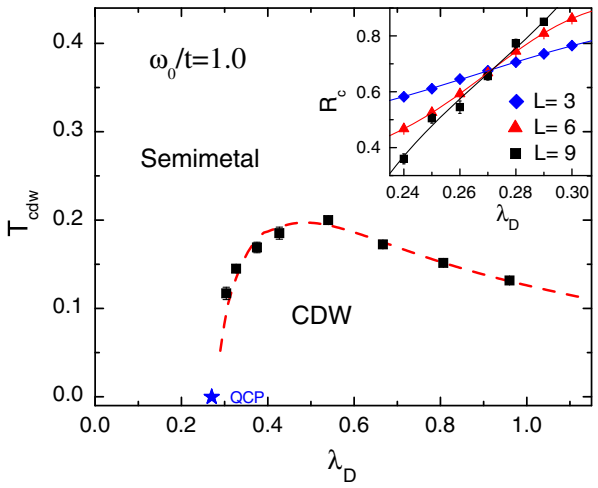

FIG. 5. Critical temperature for the CDW transition in the honeycomb Holstein model inferred from finite-size scaling analysis in Fig. 2. The inset shows the crossing of the invariant correlation ratio R_c (see text), resulting in the indicated QCP, in good agreement with the value at which an extrapolated T_c would vanish.

with order for all nonzero λ_D. On the other hand, S_{CDW} shows much less T dependence in the honeycomb case, with results from $\beta = 12$ to 20 being almost identical (within error bars).

Further insight into the existence of a critical EPC is provided by CDW gap, inferred from the plateau in $\rho(\mu)$ via $\Delta_c \equiv \mu(\rho = 1 + x) - \mu(\rho = 1 - x)$. Here we choose $x = 0.01$; other values of x give qualitatively similar results. Figure 4(a) displays Δ_c for different λ_D and fixed $\beta = 10$ and 16. The gap has a nonmonotonic dependence on the EPC, with a maximum at $\lambda_D \approx 0.43$. For smaller EPCs, the CDW gap is strongly suppressed. A crossing of the curves occurs at $\lambda_D \sim 0.27$ so that Δ_c *decreases* as T is lowered for $\lambda_D \lesssim 0.27$, consistent with a critical EPC. The compressibility $\kappa = \partial\rho/\partial\mu$ is presented as a function of λ_D in Fig. 4(b) for honeycomb and square lattices at several T. We have normalized by the noninteracting value κ_0 (evaluated in the thermodynamics limit) to provide a comparison that eliminates trivial effects of the DOS. For the honeycomb lattice, κ/κ_0 shows a sharp increase around $\lambda_D \sim 0.27 \pm 0.01$, consistent with the vanishing of S_{CDW} in Fig. 3. Furthermore, κ/κ_0 grows with β. For the square lattice, κ/κ_0 vanishes down to much smaller λ_D, behaves more smoothly at the lowest T, and is an order of magnitude smaller. Its small residual value is a consequence of the exponentially divergence of the CDW ordering temperature as $\lambda_D \to 0$.

Finally, we have obtained T_c for a range of λ_D above the critical EPC, yielding the phase diagram in Fig. 5. T_c decreases rapidly at $\lambda_D \approx 0.28$. The inset shows the crossing of the invariant correlation ratio R_c, a quantity which is independent of lattice size at a quantum critical point (QCP) (see Supplemental Material [33,34]). T_c exhibits a maximum at $\lambda_D \sim 0.4$–0.5, which lies close to the coupling for which Δ_{CDW} is greatest (Fig. 4). The maximum in T_c reflects a competition between a growth with λ_D as it induces CDW order with a reduction as the EPC renormalizes the single electron mass, yielding a heavy polaron [33,42–49]. Unlike CDW order, which arises directly from intersite interactions, in the Holstein model it is produced by a second order process: the lowering of the kinetic energy by virtual hopping between doubly occupied and empty sites. A mass renormalization-driven reduction in this hopping lowers T_c.

Conclusions.—In this Letter, we have presented DQMC simulations of the Holstein model on a honeycomb lattice. The existence of long-range charge order was established below a finite critical transition temperature in the range $T \sim t/6$, for sufficiently large EPC. T_c is similar for the square and honeycomb lattices, despite the dramatic differences in their noninteracting densities of states: diverging in the former case and vanishing in the latter.

Our data suggest that, as for the honeycomb Hubbard model [4–9], the vanishing noninteracting density of states

of Dirac fermions gives rise to a minimal value for $\lambda_D \sim (0.27 \pm 0.01)t$, only above which does LRO occur. Thus, although the critical CDW transition temperatures for the two geometries are similar when order occurs, the Dirac density of states does fundamentally alter the phase diagram by introducing a weak-coupling regime in which order is absent. The 1D Holstein model is also known to have a metallic phase for electron-phonon couplings below a critical value [50,51].

This initial study has focused on a simplified model. The phonon spectra of graphene and graphitic materials have been extensively explored [52] and, of course, are vastly more complex than the optical phonon mode incorporated in the Holstein Hamiltonian. However, as has been recently emphasized [26], including realistic phonon dispersion relations is relatively straightforward in QMC simulations, since the associated modifications affect only the local bosonic portion of the action and not the computationally challenging fermionic determinants. One important next step will be the study of more complex phonon modes and the types of electronic order and phase transitions that they induce. Such investigations open the door to examining hexagonal CDW materials like the transition-metal dichalcogenides [53–56]. However, their layered structures add considerable challenges to descriptions with simple models.

The work of Y.-X. Z., W.-T. C., and R. T. S. was supported by the Department of Energy under Award No. DE-SC0014671. G. G. B. is partially supported by the French government, through the UCAJEDI Investments in the Future project managed by the National Research Agency (ANR) with Reference No. ANR-15-IDEX-01. N. C. C. was supported by the Brazilian funding agencies CAPES and CNPq.

Note added.—Recently, we learned of a related investigation by Chen *et al.* [57].

*zyxzhang@ucdavis.edu

[1] A. Geim and K. Novoselov, Nat. Mater. **6**, 183 (2007).
[2] A. Black-Schaffer and C. Honerkamp, J. Phys. Condens. Matter **26**, 423201 (2014).
[3] B. Wunsch, F. Guinea, and F. Sols, New J. Phys. **10**, 103027 (2008).
[4] T. Paiva, R. T. Scalettar, W. Zheng, R. R. P. Singh, and J. Oitmaa, Phys. Rev. B **72**, 085123 (2005).
[5] Z. Meng, T. Lang, S. Wessel, F. Assaad, and A. Muramatsu, Nature (London) **464**, 847 (2010).
[6] B. K. Clark, D. A. Abanin, and S. L. Sondhi, Phys. Rev. Lett. **107**, 087204 (2011).
[7] S. Sorella, Y. Otsuka, and S. Yunoki, Sci. Rep. **2**, 992 (2012).
[8] F. F. Assaad and I. F. Herbut, Phys. Rev. X **3**, 031010 (2013).
[9] Y. Otsuka, S. Yunoki, and S. Sorella, Phys. Rev. X **6**, 011029 (2016).
[10] A. M. Black-Schaffer and S. Doniach, Phys. Rev. B **75**, 134512 (2007).
[11] R. Nandkishore, L. Levitov, and A. Chubukov, Nat. Phys. **8**, 158 (2012).
[12] C. Honerkamp, Phys. Rev. Lett. **100**, 146404 (2008).
[13] W.-S. Wang, Y.-Y. Xiang, Q.-H. Wang, F. Wang, F. Yang, and D.-H. Lee, Phys. Rev. B **85**, 035414 (2012).
[14] M. L. Kiesel, C. Platt, W. Hanke, D. A. Abanin, and R. Thomale, Phys. Rev. B **86**, 020507 (2012).
[15] S. Pathak, V. B. Shenoy, and G. Baskaran, Phys. Rev. B **81**, 085431 (2010).
[16] T. Ma, Z. Huang, F. Hu, and H.-Q. Lin, Phys. Rev. B **84**, 121410 (2011).
[17] Z.-C. Gu, H.-C. Jiang, D. N. Sheng, H. Yao, L. Balents, and X.-G. Wen, Phys. Rev. B **88**, 155112 (2013).
[18] S. Jiang, A. Mesaros, and Y. Ran, Phys. Rev. X **4**, 031040 (2014).
[19] X. Y. Xu, S. Wessel, and Z. Y. Meng, Phys. Rev. B **94**, 115105 (2016).
[20] T. O. Wehling, E. Şaşıoğlu, C. Friedrich, A. I. Lichtenstein, M. I. Katsnelson, and S. Blügel, Phys. Rev. Lett. **106**, 236805 (2011).
[21] I. F. Herbut, Phys. Rev. Lett. **97**, 146401 (2006).
[22] G. Grüner, Rev. Mod. Phys. **60**, 1129 (1988).
[23] G. Grüner, *Density Waves in Solids* (Addison-Welsley, Reading, MA, 1994), Vol. 89.
[24] N. C. Costa, W. Hu, Z. J. Bai, R. T. Scalettar, and R. R. P. Singh, Phys. Rev. B **96**, 195138 (2017).
[25] M. Weber and M. Hohenadler, Phys. Rev. B **98**, 085405 (2018).
[26] N. C. Costa, T. Blommel, W.-T. Chiu, G. Batrouni, and R. T. Scalettar, Phys. Rev. Lett. **120**, 187003 (2018).
[27] F. Marsiglio, Phys. Rev. B **42**, 2416 (1990).
[28] M. Vekic, R. M. Noack, and S. R. White, Phys. Rev. B **46**, 271 (1992).
[29] H. Zheng and S. Y. Zhu, Phys. Rev. B **55**, 3803 (1997).
[30] T. Holstein, Ann. Phys. (N.Y.) **8**, 325 (1959).
[31] R. Blankenbecler, D. J. Scalapino, and R. L. Sugar, Phys. Rev. D **24**, 2278 (1981).
[32] M. Creutz and B. Freedman, Ann. Phys. (N.Y.) **132**, 427 (1981).
[33] See Supplemental Material http://link.aps.org/supplemental/10.1103/PhysRevLett.122.077602 for more details about (i) the Holstein model, (ii) the DQMC Algorithm, (iii) the Binder ratio, and (iv) critical exponents, as well as physical quantities such as (v) electron kinetic energy, (vi) double occupancy, (vii) CDW gap, and (viii) correlation length, which includes Refs. [31,34–37].
[34] K. Binder, Z. Phys. B **43**, 119 (1981).
[35] A. Sandvik (private communication).
[36] S. R. White, D. J. Scalapino, R. L. Sugar, E. Y. Loh, J. E. Gubernatis, and R. T. Scalettar, Phys. Rev. B **40**, 506 (1989).
[37] O. Melchert, arXiv:0910.5403.
[38] G. G. Batrouni and R. T. Scalettar, Phys. Rev. B **99**, 035114 (2019).
[39] S. Blawid and A. J. Millis, Phys. Rev. B **63**, 115114 (2001).
[40] J. K. Freericks, M. Jarrell, and D. J. Scalapino, Phys. Rev. B **48**, 6302 (1993).
[41] R. Peierls, *Quantum Theory of Solids* (Oxford University, New York, 1955).
[42] E. Jeckelmann and S. R. White, Phys. Rev. B **57**, 6376 (1998).

[43] J. Bonča, S. A. Trugman, and I. Batistić, Phys. Rev. B **60**, 1633 (1999).
[44] A. H. Romero, D. W. Brown, and K. Lindenberg, Phys. Rev. B **60**, 14080 (1999).
[45] L.-C. Ku, S. A. Trugman, and J. Bonča, Phys. Rev. B **65**, 174306 (2002).
[46] P. E. Kornilovitch, Phys. Rev. Lett. **81**, 5382 (1998).
[47] M. Hohenadler, H. G. Evertz, and W. von der Linden, Phys. Rev. B **69**, 024301 (2004).
[48] A. Macridin, G. A. Sawatzky, and M. Jarrell, Phys. Rev. B **69**, 245111 (2004).
[49] G. L. Goodvin, M. Berciu, and G. A. Sawatzky, Phys. Rev. B **74**, 245104 (2006).
[50] E. Jeckelmann, C. Zhang, and S. R. White, Phys. Rev. B **60**, 7950 (1999).
[51] M. Hohenadler and H. Fehske, Eur. Phys. J. B **91**, 204 (2018).
[52] L. Karssemeijer and A. Fasolino, Surf. Sci. **605**, 1611 (2011).
[53] X. Zhu, Y. Cao, J. Zhang, E. W. Plummer, and J. Guo, Proc. Natl. Acad. Sci. U.S.A. **112**, 2367 (2015).
[54] C. J. Arguello, S. P. Chockalingam, E. P. Rosenthal, L. Zhao, C. Gutiérrez, J. H. Kang, W. C. Chung, R. M. Fernandes, S. Jia, A. J. Millis, R. J. Cava, and A. N. Pasupathy, Phys. Rev. B **89**, 235115 (2014).
[55] J. Dai, E. Calleja, J. Alldredge, X. Zhu, L. Li, W. Lu, Y. Sun, T. Wolf, H. Berger, and K. McElroy, Phys. Rev. B **89**, 165140 (2014).
[56] W. Sacks, D. Roditchev, and J. Klein, Phys. Rev. B **57**, 13118 (1998).
[57] C. Chen, X. Y. Xu, Z. Y. Meng, and M. Hohenadler, preceding Letter, Phys. Rev. Lett. **122**, 077601 (2019).